

Rain observations with a vertically looking Micro Rain Radar (MRR)

Gerhard Peters¹⁾, Bernd Fischer¹⁾ and Tage Andersson²⁾

¹⁾ *Meteorologisches Institut, Universität Hamburg, Bundesstrasse 55, D-20146 Hamburg, Germany*

²⁾ *Swedish Meteorological Society, Skolmästarweg. 59, SE-60176 Norrköping, Sweden*

Peters, G., Fischer, B. & Andersson, T. 2002: Rain observations with a vertically looking Micro Rain Radar (MRR). — *Boreal Env. Res. 7*: 353–362. ISSN 1239-6095

Measurements of rain were obtained with a vertically pointing micro radar (MRR) with 1 min time resolution and 50(100) m height resolution at the German Baltic coast on the Zingst peninsula (54.43°N, 12.67°E). The comparison with a conventional rain gauge (30 min integration time) for a five months summer period show a correlation coefficient of $\rho = 0.87$ for the rainrate and agreement within 5% for the total rainfall integrated over the whole period. Single measurements with 30 min integration time showed deviations up to a factor of 2 between MRR and rain gauge. Classification of the measurements into rainrate intervals shows that rainrates around 0.2 mm h^{-1} provide the highest contribution per rainrate interval to the total rainfall. Typical distributions of number-concentration, liquid-water- concentration and rainrate versus drop size, retrieved with the MRR, are presented. Simultaneous estimates of rainrate and reflectivity factor with data of a C-band (frequency 6 GHz) weather radar suggest that the MRR may be used to support quantitative rainrate estimates with weather radars. The weather radar used for comparison is operated by the German Weather Service and is situated 51 km from the MRR.

Introduction

Improvement of the present quality of precipitation measurement is important to achieve progress in our understanding of the hydrological cycle — the main goal of BALTEX (Baltic Sea Experiment) and GEWEX (Global Energy and Water Cycle Experiment). This is the motivation for the development of a variety of technologies ranging from global satellite borne observation methods to new surface *in-situ* instruments. The

retrieval of areal quantitative precipitation from conventional weather radars suffers from mainly two problems:

- The relation between the radar reflectivity and rainrate depends on the structure of the drop size distribution. Parameterized distributions can deviate considerably from actual distributions. Richter and Hagen (1997) demonstrated that this problem can be mitigated by advanced radar techniques including for example polarimetry.

- The height of the measuring volume increases with increasing distance from the radar due to the earth curvature. In moderate zones the majority of weather radar data are obtained above the freezing level. Stratiform shallow rainclouds may be totally below the sampling height of the radar. In general the extrapolation from the radar measuring volume to the surface includes significant uncertainties.

Here we report results obtained with a vertically looking Micro-Rain-Radar (MRR) which was installed in the frame of PEP (Precipitation and Evaporation Project), supported by EU under contract ENV4-CT97-0484 at the German Baltic coast on the Zingst peninsula. The system is in operation continuously since 1998. Unlike conventional weather radars the MRR does not provide areal coverage as it is operated only as a vertically looking profiler. The advantage of this operation mode is that the measured Doppler spectra can be transformed into number concentration versus drop size using the known relation between drop size and terminal fall velocity as suggested already by Atlas *et al.* (1973). From the drop size distributions various microphysical parameters and the rainrate can be estimated without any assumption about the form of the drop size distributions. As all results are available as functions of measuring height they can be used to link weather radar measurements from aloft to the actual surface conditions.

Retrieval of microphysical distributions and parameters

The MRR is a FM-CW (Frequency Modulated Continuous Wave) Doppler radar with a parabolic offset dish with 0.5 m efficient aperture diameter and 24.1 GHz transmit frequency. The CW-operation makes optimum use of the available transmit power. Thus a stable and reliable Gunn oscillator with only 50 mW output power can be used for the transmitter. The retrieval of range-resolved Doppler spectra follows the method described by Strauch (1976).

The spectral volume reflectivity $\eta(f)$ as a function of Doppler frequency f is related to the

spectral power $p(r,f)$, received by the radar from a range gate centered at r with the depth δr under the condition $\delta r/r \ll 1$, by

$$\eta(r, f)df = p(r, f)df \cdot C \frac{r^2}{\delta r} t^{-1}(r) \quad (1)$$

where C is a constant containing radar specific parameters as for example transmit power and antenna gain. It was determined by the manufacturer before installation at the test site. The transmission $t(r)$ is the fraction of the power of a plane wave which penetrates a layer of thickness r . $t(r)$ is mainly related to the scattering at rain drops and was calculated with Mie theory by a recursive method starting with the drop size distribution in the lowest range gate, which is retrieved using Eq. 1 with the assumption $t(r_1) = 1$. Other effects on the transmission were neglected.

To be consistent with conventional weather radar terminology the “equivalent spectral radar reflectivity factor”

$$z_e df = \frac{\eta(f)df}{\left(\frac{\pi^5}{\lambda^4}\right) |K^2|} \quad (2)$$

is introduced with $|K^2| \approx 0.92$. Within the Rayleigh approximation ($D \ll \lambda$) the integral $Z_e = \int z_e df$ is identical with the usual radar reflectivity factor Z , defined in Eq. 7.

The drop size distribution $n(D)$ is calculated using the relation between volume reflectivity $\eta(D)$ and single particle scattering cross section $\sigma(D)$:

$$n(D) = \frac{\eta(D)}{\sigma(D)} \quad (3)$$

$\sigma(D)$ is calculated by Mie-theory, and $\eta(D)$ is related to the measured spectral reflectivity $\eta(f)$ by

$$\eta(D) = \eta(f) \frac{\partial f}{\partial v} \frac{\partial v}{\partial D} \quad (4)$$

where $\partial f/\partial v$ is the Doppler relation, $\partial v/\partial D = -6.18 \exp(-0.6 \text{ [mm]}) (\rho_0/\rho)^{0.4}$ is an analytical fit to an empirical relation found by Gunn and Kinzer (1949), and $(\rho_0/\rho)^{0.4}$ describes the influence of air density on the fall velocity. The influence of vertical wind and turbulence was

neglected here, which represents probably the most important source of error of this method (e.g. Joss and Dyer, 1972, Richter, 1994).

On the basis of $n(D)$ the liquid water content distribution

$$lwc(D) = \frac{\pi}{6} \rho_w D^3 n(D) \quad (5)$$

with ρ_w = water density and the rainrate distribution

$$rr(D) = \frac{\pi}{6} D^3 v(D) n(D) \quad (6)$$

is calculated.

Integration of Eqs. 3–6 over D yields the number concentration N , the volume backscatter cross section η , the liquid water content LWC and the rainrate R , respectively.

For comparison of the measured values of η with weather radar reflectivities it must be taken into account, that the scattering cross section at the weather radar wave length ($\lambda_{wr} \approx 5$ cm) is well described by the Rayleigh approximation. Therefore, the integral

$$Z = \int n(D) D^6 dD \quad (7)$$

is calculated, which represents the radar reflectivity factor in the Rayleigh approximation, and corresponds directly to the weather radar output.

In addition, the first moment of the Doppler spectrum is calculated and is referred to as mean fall velocity v_m .

$$v_m = \frac{\lambda}{2} \frac{\int p(f) f df}{\int p(f) df} \quad (8)$$

Although the relation between v_m and the Doppler spectrum is very straightforward, v_m might be not the best choice to characterize “rainfall velocity” as it is weighted in a complex way with respect to the droplet fall velocity distribution due to the non-linear dependence of σ and v on D . Qualitatively, it represents primarily the velocity of larger drops. Other physically more obvious weightings (e.g. $\propto lwc(D)$) could be designed.

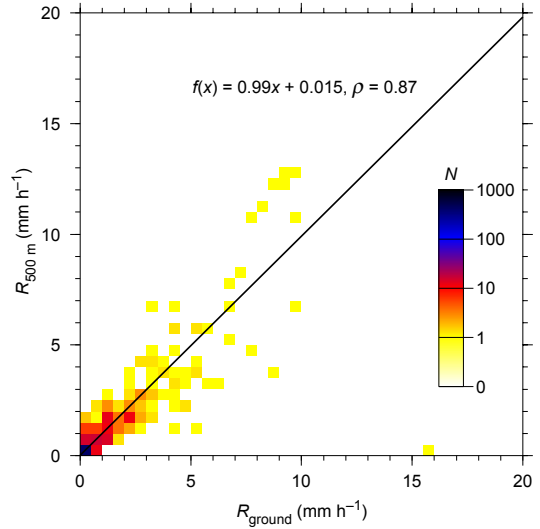


Fig. 1. Frequency diagram MRR rainrate at 500 m height versus rain gauge, 30 min averages on the Zingst peninsula (May–September 1998).

Comparison of rain measured rates

A five months measuring period from May to September 1998 was selected for comparison. During this time the assumption of liquid precipitation, which is necessary for the retrieval algorithm, was justified at least in the lower parts of the radar profiles. A THIES rain gauge is operated by the Umweltbundesamt in the vicinity of the MRR. The rain gauge issues one pulse per 0.1 mm rainfall, and the integration time of the data is $\Delta_t = 30$ min. Thus the rainrate estimates R from the rain gauge are multiples of $\Delta_r = \Delta_f / \Delta_t$, mm h^{-1} . For better comparison the MRR rainrates were also averaged over 30 min and all data were classified into 0.5 mm h^{-1} classes. The height resolution of the radar was set to 50 m, and the 10th range gate corresponding to 500 m height was selected as a compromise between minimizing the distance rain gauge — scattering volume and satisfying the condition $(\delta r)/r \ll 1$. Figure 1 is a 2-dimensional histogram showing the number of events in 2-dimensional classes of $0.5 \text{ mm h}^{-1} \times 0.5 \text{ mm h}^{-1}$ width. Since neither the rain-gauge nor the radar represent an absolute reference, we did not declare one or the other output as

independent variable for calculating the slope of the linear regression. Instead of this the slope of the regression was identified with the ratio of the standard deviations of both data sets. The correlation coefficient 0.87 and the slope 0.99 indicate a good general agreement of both instruments.

Only samples where at least one of both instruments detected rain were included in the comparison. This represents about 12% of the total time or 906 samples with rain, each sample spanning 30 min integration time. Two third of all samples falls in the lowest class (0–0.5 mm h⁻¹). One case with anomalous Doppler spectra and extremely high apparent MRR-rainrates persisting 30 min needs further investigation and was excluded from the comparison. There is one further suspicious event to be seen in the histogram at 16 mm h⁻¹ rain gauge rainrate and 0 mm h⁻¹ radar rainrate, which was not discarded.

A look on statistics of rainfall

Precipitation exhibits an extremely strong temporal and spatial variability in a wide range of scales. This feature makes the direct comparison between model results and measurements particularly difficult. An easier way to assess the quality of models is for example to compare statistical characteristics of model results with those of observed data. A prerequisite for the measurements in this application is that the corresponding statistics are not distorted due to insufficient instrumental resolution.

In this section we will show that conventional rain gauge data suffer severely from such distortions and that MRR measurements are superior in this respect.

Comparison of resolution

The most striking difference between rain measurements with a conventional rain gauge and the MRR respectively is related to the resolution of time and rainrate.

The primary variable observed with a rain gauge is the rainfall F , and the resolution Δ_F of this variable is a fixed system parameter as

mentioned previously. Therefore, the rainrate-resolution is inversely proportional to the time-resolution

$$\Delta_R = \frac{\Delta_F}{\Delta_t} \quad (9)$$

The relation between rainrate- and time-resolution for the MRR is more involved than Eq. 9 and its discussion would be beyond the scope of this paper. But the minimum detectable rainrate can be determined empirically by measuring the corresponding signal to noise ratio which must exceed a certain threshold. At 1000 m height and for 1 min averaging time a minimum detectable “rainrate” $\Delta_R = 0.01$ mm h⁻¹ was found. The signs of quotation are used as such low intensities may be more adequately termed “drizzle” or “cloud”.

To illustrate the difference: While the MRR can measure a rainrate of 0.1 mm h⁻¹ comfortably and with reasonable accuracy within 1 min time-resolution, the rain gauge would need 1 hour to collect sufficient water for just 1 impulse. In reality the rain gauge output would still be meaningless in such a situation.

Distribution of rainrates

One basic statistical feature of rain is the contribution of rainrates to the total rainfall within the whole analysis time (5 months in this case). The cumulative distribution, i.e. the rainfall $F(R,t)$ due to rainrates less than R during the time period t , is given by

$$F(R,t) = \int_0^t x(t') dt' \quad (10)$$

with $x = \begin{cases} \text{rainrate} & \text{if } x \leq R \\ 0 & \text{otherwise} \end{cases}$

In a first step $F(R,t)$ was calculated on the basis of 30 min averages for the rain gauge as well as for the MRR and after classification of the rainrate in intervals of 0.25 mm h⁻¹ (Fig. 2). Again 500 m measuring altitude has been used for the MRR. The right end of the distributions represents the total rainfall which agrees within 5 for both instruments. Not only the total rainfall but also the shapes of the distributions agree quite well. The cumulative distributions reach saturation at about $R = 10$ mm h⁻¹ indicating that

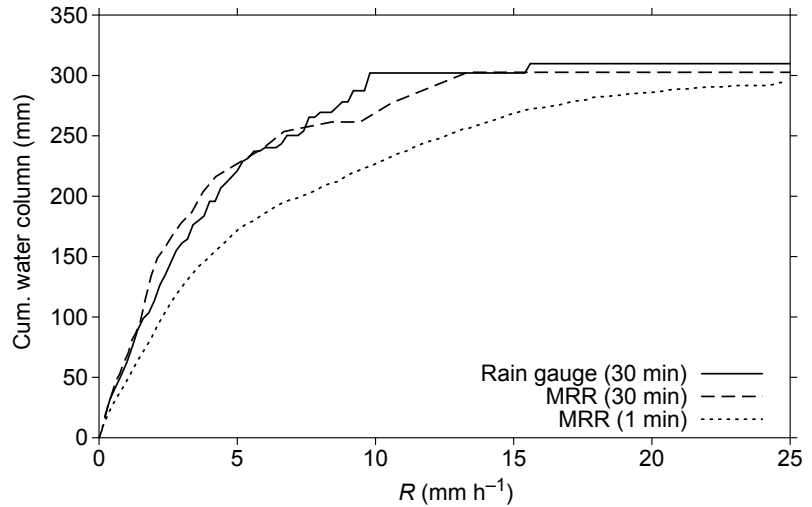


Fig. 2. Cumulative contribution of rainrates to the total rainfall on the Zingst peninsula (May–September 1998).

only few events occurred with stronger rainrates.

In a second step the original 1 min MRR data were used to calculate $F(R,t)$ (dotted line in Fig. 2). While the total rainfall has not changed significantly (except of slight effects due to few events exceeding 25 mm h^{-1}) one recognizes that the frequency of high rainrates has increased considerably on the expense of low rainrates. The reason for this shift is, that the duration of most rain events is shorter than 30 min. In these cases the averaging process causes an underestimation of the actually occurring rainrates. A comprehensive study of rain- and drought-durations in this data set can be found in Peters *et al.* (2002).

The results do not prove that 1 min time resolution is sufficient to reveal the true distribution of rainrates, but it is obvious that the results are more faithful than based on 30 min averages.

Inspection of the $F(R,t)$ shows, that its slope is steepest for the lowest rainrate. That means that the lowest rainrate class ($0\text{--}0.25 \text{ mm h}^{-1}$) contributes most to the total rainfall. This is no artifact caused by excessive integration time, as it is even true for the 1 minute distribution. Therefore, shortening of the integration time is not allowed for the rain gauge used here as it would introduce significant distortions at the left tail of the rainrate distribution due to the loss of rainrate resolution according to Eq. 9.

In order to find out, whether or not there is any lowest “significant” rainrate, the frequency

distribution of rainrates was calculated (averages of 1 min for MRR and 30 min for the rain gauge). In order to achieve adequate resolution of small rainrates a logarithmic scale was chosen for the abscissa. In case of the MRR equidistant classes on the logarithmic scale were chosen ($\Delta R/R = 0.05$). The rainfall found in each class was divided by the corresponding class-width in order to eliminate the influence of the individual class width. The result — termed “differential water column” in units $\text{mm}/(\text{mm h}^{-1})$ — is shown on the left side of Fig. 3. The maximum contribution to the total rainfall stems from rainrates around 0.2 mm h^{-1} , which would be far below the resolution of rain gauges for this averaging time. For comparison the corresponding distribution is shown for the rain gauge data on the right side of Fig. 3. Due to the discrete output of the instrument a linear constant classwidth ($\Delta R = 0.2 \text{ mm h}^{-1}$ centered at multiples of 0.2 mm h^{-1}) was chosen here. Again the rainfall in each class was divided by the (constant) class width. By this operation the ordinate values of both distributions are comparable. Here the maximum occurs at the lowest class. From this position of the maximum one can only infer that the highest rainfall contribution stems from rainrates $\leq 0.3 \text{ mm h}^{-1}$. I.e. the resolution of the rain gauge is not sufficient to identify the most important rainrate class. (For 30 min averages the peak position would appear at rainrates $\ll 0.2 \text{ mm h}^{-1}$, which can be shown by averaging the MRR data.)

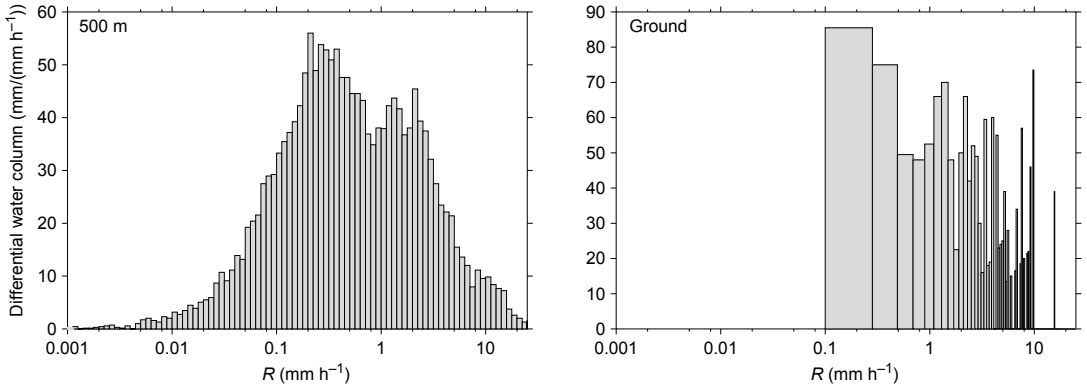


Fig. 3. Histogram of rainrates, normalized with the class-width, versus logarithm of rainrate. Left: MRR on (Zingst peninsula May–September 1998), Right: rain gauge (Zingst peninsula May–September 1998). See text for details.

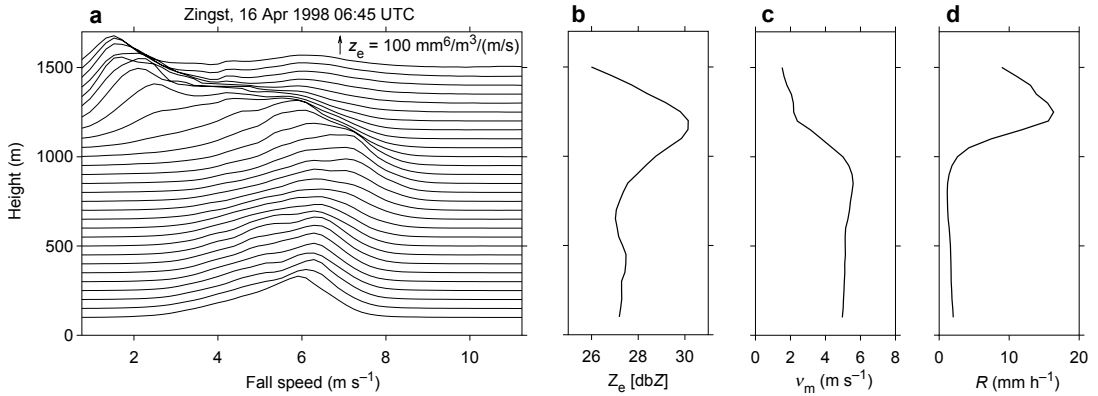


Fig. 4. — **a:** Waterfall presentation of raw Doppler spectra of radar reflectivity averaged over 1 min from 100 to 1500 m. The height resolution is 50 m. The z_e -calibration is given by the arrow in top of the figure. — **b:** Profiles of radar reflectivity Z_e . — **c:** Mean fall velocity v_m . — **d:** Rainrate R . — The melting level at 1100 m appears as a peak of Z_e (bright band), as a step of v_m and as a peak of the apparent rainrate R respectively.

Profiles and spectra

Figure 4a shows a waterfall presentation of the spectral radar reflectivity z_e versus Doppler frequency f as defined in Eq. 2 for all range gates in one selected minute in April 1998. The spectral peak in the lower range gates is at about 6 m s⁻¹. At heights above 1100 m (the melting level at this time) the spectral peak is shifted to 2 m s⁻¹ and becomes fairly narrow which is typical for snow fall, as also other researchers have found, see for instance Gossard *et al.* (1990) or Duvernoy and Gaumet (1996). The corresponding profiles of radar reflectivity Z_e , mean fall velocity v_m and rainrate R are shown in Fig. 4b–d).

The melting level appears in these profiles as enhanced reflectivity, as step in fall velocity, and as apparently enhanced rainrate, respectively. The last feature is an artifact, as the retrieval is only applicable for the liquid phase. Nevertheless it can be used as sensitive indicator for the melting level, even when it is not detectable in the reflectivity profile. These profiles, showing the melting level, may be used to identify the state of precipitation, rain or snow. This information could be helpful also for the interpretation of weather radar data.

In Fig. 5a–e typical microphysical distributions derived from Doppler spectra during stratiform rain in three subsequent minutes are pre-

sented for the level of 100 m. The rainrate was fairly constant (4.8 to 5.0 mm h⁻¹). The vertical lines in the raw Doppler spectra $z_e(f)$ (Fig. 5a) indicate limits of the analysis range which were introduced to avoid instabilities of the retrieval algorithm (Richter 1994). At the first glance some significant contribution seems to be lost at the upper end of the spectrum. The figures below illustrate that this is not the case. The spectral peak of $z_e(v)$ appears at about 6.2 m s⁻¹, which corresponds to drops with 1.8 mm diameter. In Fig. 5b, z_e is plotted as a function of drop diameter D . Due to the non-linear Gunn-Kinzer relation it appears that the spectrum is distorted with more weight on the left hand side, consequently the peak diameter is shifted to 1.6 mm. With Eq. 3 the drop size distribution $n(D)$ was calculated as shown in Fig. 5c. The thin dotted lines in Fig. 5c–e represent the exponential fit of Eq. 11, suggested by Marshall and Palmer (1948), to the drop size distribution for the actual mean rainrate mm h⁻¹.

$$N(D) = N_0 \exp(-\Lambda D) \quad (11)$$

with $\Lambda = 4.1(R [\text{mm h}^{-1}])^{-0.21} \text{ mm}^{-1}$ and $N_0 = 8 \times 10^3 \text{ m}^{-3} \text{ mm}^{-1}$. The flattening of the measured distributions at $D = 1 \text{ mm}$ is qualitatively consistent with observations of Laws and Parsons (1943), and the steeper slope for $D < 1 \text{ mm}$ is expected in theoretical stationary distributions calculated by Srivastava (1971). These seemingly small structures correspond to a strong variability of the liquid-water- and rainrate-distributions (Fig. 5d and e) in the small droplet range, causing bimodal distributions. Although the left lwc-peak is highest in two samples the corresponding contribution to the rainrate is less pronounced due to the smaller fall velocity of smaller drops. The peak contribution to the rainrate is produced in all three samples by drops with diameters around 1.3 mm in agreement with the M-P-based

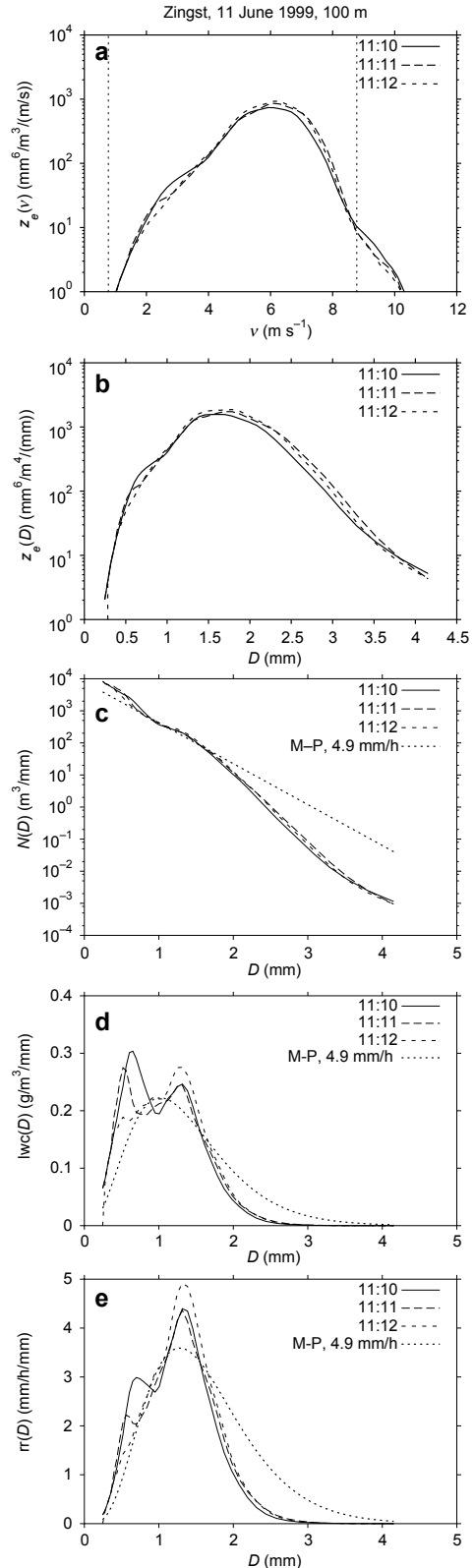


Fig. 5 (right). — **a**: Spectral radar reflectivity factor as function of Doppler velocity. — **b–e**: Various functions of drop diameter: — **b**: radar reflectivity factor, — **c**: number density, — **d**: liquid water concentration, — **e**: Rain rate. The dotted lines in **c–e** indicate the corresponding functions assuming a M-P drop size distribution for the rain rate 4.9 mm h⁻¹.

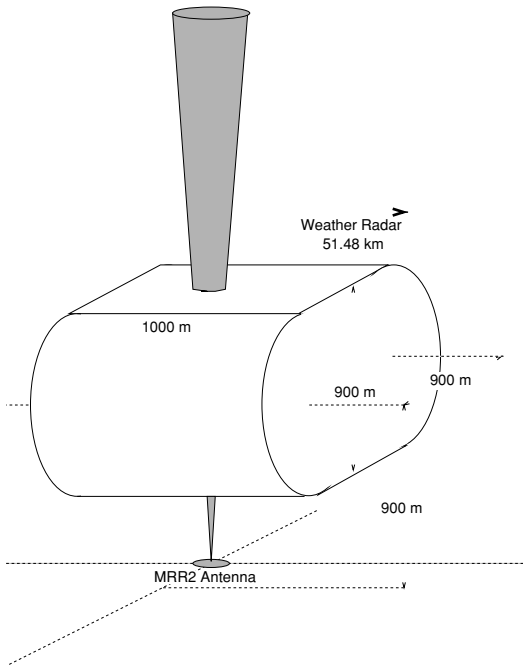


Fig. 6. Position and shape of MRR- and weather-radar-scattering-volume.

distribution, but the measured rainrate is weaker for large drops and stronger for small drops than the M-P-based distribution. In these examples contributions from drops with $D > 4$ mm corresponding to 8.7 m s^{-1} fall velocity can be safely neglected, which is true in most cases. Few observed exceptions were probably related to hail (not shown here), where the retrieval algorithm can not be used anyway. Therefore, the above mentioned truncation of the spectra at 9.36 m s^{-1} is justified.

Weather radar comparison

Weather radar data from two days in July 2000 with a total rain duration of 9 h and a sampling period of 5 min were provided by Deutscher Wetterdienst (DWD) for comparison. The weather radar is located in 51.48 km distance from the MRR. The lowest weather radar measuring volume over the MRR is centered at 900 m altitude. It has 900 m diameter and 1000 m length and can be approximated by a horizontally oriented cylinder of 900 m diameter. Two

subsequent samples of the weather radar scan, which fitted best the position of the MRR, were averaged for comparison. Due to the continuous azimuth rotation of the radar antenna the horizontal cross-beam extension of the effective scattering volume is about 1800 m. For further improvement of the comparability the MRR-data were averaged also between 500 and 1400 m. The vertical resolution of the MRR was set to 100 m for this comparison. The scattering volume geometries are sketched in Fig. 6. Figure 7a and b show time height cross sections of rain rates for both days. Note that the time axes are different. The melting layer, showing up as a marked apparent rainrate maximum, is always around 2400 m, so that the comparison volume is entirely below the melting layer. In Fig. 8 the radar reflectivity Z_{MRR} , calculated with Eq. 7, is compared with the weather radar output Z_{WR} . The mean bias was removed by adjustment of the MRR since, due to replacement of a receiver component, the MRR was not calibrated at this time. Not all fine structures observed by the MRR appear in the weather radar data because the weather radar sampling period was 5 min in contrast to 1 min of the MRR. Reflectivities below -5 dBZ are missing in weather radar data probably because they fall below the detection threshold.

Nevertheless, the variation of the measured reflectivity factors in the common scattering volume agrees well enough, thus that it appears possible to use such simultaneous measurements for continuously updating the actual Z - R -relation. In addition, this example shows how the weather radar measurements could be linked to the rainfall at the surface by use the MRR-profiles. In this particular example the mean rainrate profile shows a significant gradient. The rainrate, averaged over the whole time period at 500 m, exceeds the corresponding value at 1400 m by a factor 1.5.

Of course, it must be kept in mind that any areal extrapolation of local rain characteristics is generally not straightforward.

Summary and outlook

First long term experiences with a vertically pointing micro rain radar MRR showed good

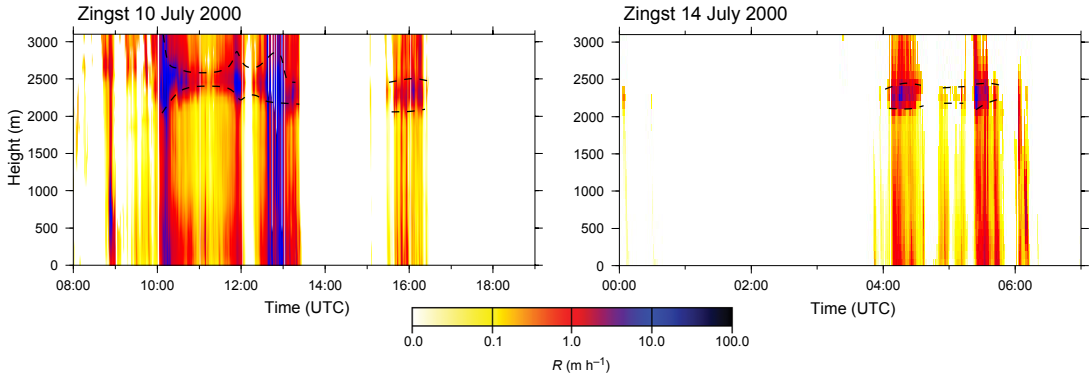


Fig. 7. Time-height cross section of rainrate derived with Eq. 6 during the time periods used for the weather radar comparison. The melting layer shows an apparent enhancement of rain rate; the boundaries are indicated by dashed lines.

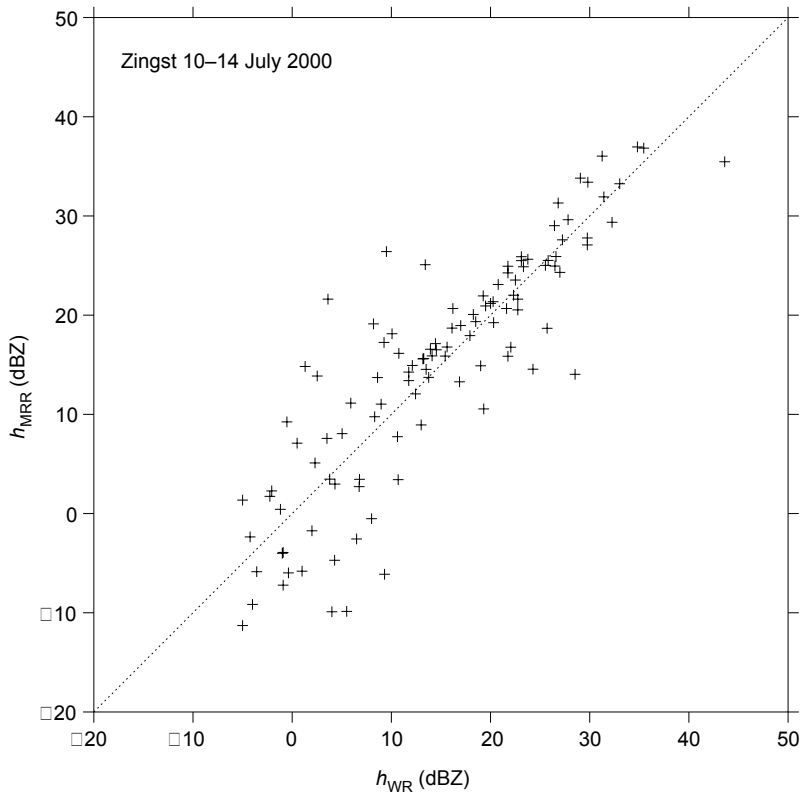


Fig. 8. Comparison of radar reflectivity factor, calculated in Rayleigh approximation with Eq. 11, with weather radar output.

correlation with conventional rain gauge measurements. It was found that weak rainrates ($\approx 0.2 \text{ mm h}^{-1}$) yield the highest contribution to the total rainfall. Although this may be specific for the local climate conditions, it underlines that rain measurements with finer resolution than of conventional rain gauges are necessary to obtain

a realistic presentation of rainfall distributions. Comparisons with simultaneous weather radar data suggest a potential application: The support of weather radar operation for retrieval of quantitative rainfall.

One limitation of the applied drop size retrieval has not been addressed in this paper,

that is the error caused by non-zero vertical wind including turbulence. It is certainly of concern in convective rain, and is a main issue of further development of this method. The feasibility of available estimation methods (e.g. Probert-Jones and Harper 1962, Hauser and Amayenc 1984, Klaassen 1988) and the remaining uncertainty is investigated in an ongoing validation experiment.

The solution of the vertical wind problem may be particularly important in climate regimes with more convective situations. It is further desirable to develop quantitative retrieval algorithms for the various solid forms of precipitation.

Acknowledgments: The MRR is operated at the Umweltbundesamt (UBA) Aussenstelle Zingst with kind permission of the Umweltbundesamt. We are grateful to B. Thees and his staff for taking care of the equipment. The authors wish also to thank J. Seltmann/DWD for selecting and preparing the weather radar data.

References

- Atlas D., Srivastava R. & Sekhon R. 1973. Doppler radar characteristics of precipitation at vertical incidence. *Rev. Geophys. Space Phys.* 11: 1–35.
- Duvernoy J. & Gaumet J.L. 1996. Precipitating hydrometeor characterization by a CW Doppler Radar. *J. Atmos. Ocean. Technol.* 13: 620–629.
- Gossard E.E., Strauch R.G. & Rogers R.R. 1990. Evolution of drop size distributions in liquid precipitation observed by a ground-based Doppler radar. *J. Atmos. Ocean. Technol.* 7: 815–828.
- Gunn R. & Kinzer G. 1949. The terminal fall velocity of fall for water droplets in stagnant air. *J. Meteorol.* 6: 243–248.
- Hauser D. & Amayenc P. 1984. Raindrop-size distributions and vertical air motions as inferred from zenith pointing Doppler radar with the RONSARD system. *Radio Sci.* 19: 185–192.
- Joss, J. & Dyer R. 1972. *Large errors involved in deducing drop size distributions from Doppler radar data due to vertical air motion*, 15th Radar Meteorology Conf., Amer. Meteor. Soc., pp. 179–180.
- Klaassen W. 1988– Radar observations and simulation of the melting layer of precipitation. *J. Atmos. Sci.* 45: 3741–3753.
- Laws J.O. & Parsons D.A. 1943. The relationship of raindrop size to intensity. *Trans. Am. Geophys. Union* 24: 452–460.
- Marshall J.S. & Palmer W. 1948. The distribution of raindrops with size. *J. Meteorol.* 5: 165–166.
- Peters O., Hertlein C. & Christensen K. 2002. A complexity view of rainfall. *Phys. Rev. Letter* 88: 018701-1–018701-4.
- Probert-Jones J. & Harper W. 1962. *Vertical air motion in showers as revealed by Doppler radar*, 9th Weather Radar Conf., Amer. Meteor. Soc., pp. 225–232.
- Richter C. 1994. Niederschlagsmessungen mit dem vertikal ausgerichteten FM-CW-Dopplerradar-RASS-System, Validierung und Anwendung, Dissertation Universität Hamburg. *Berichte aus dem Zentrum für Meeres- und Klimaforschung* Nr. 12, 143 pp.
- Richter C. & Hagen M. 1997. Drop size distributions of raindrops by polarization radar and simultaneous measurements with distrometer and PMS probes. *Quarterly J. Royal Meteor. Soc.* 123: 2277–2296.
- Srivastava R.C. 1971. Size distributions of raindrops generated by their breakup and coalescence. *J. Atmos. Sci.* 28: 410–415.
- Strauch R.G. 1976. *Theory and application of the FM-CW Doppler radar*. Ph.D. thesis, Electrical Engineering, University of Colorado, 97 pp.

Received 23 January 2002, accepted 5 October 2002